# Dipole beamline

**Characteristics of the beamline**

| | |
|---|---|
| Energy range | 80 - 1500 eV |
| Flux | up to $10^{11}$ photons/s/100 mA |
| Resolving power | up to 11000 at ~400eV |
| Polarisation | Linear horizontal |
| Experimental station | fixed, RGBL-PES |

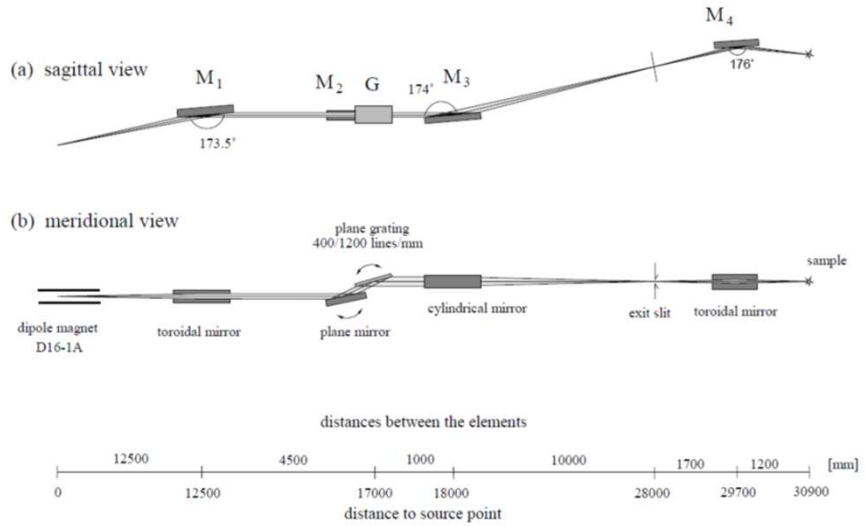


*S.I. Fedoseenko et al. / Nuclear Instruments and Methods in Physics Research A 505 (2003) 718–728*

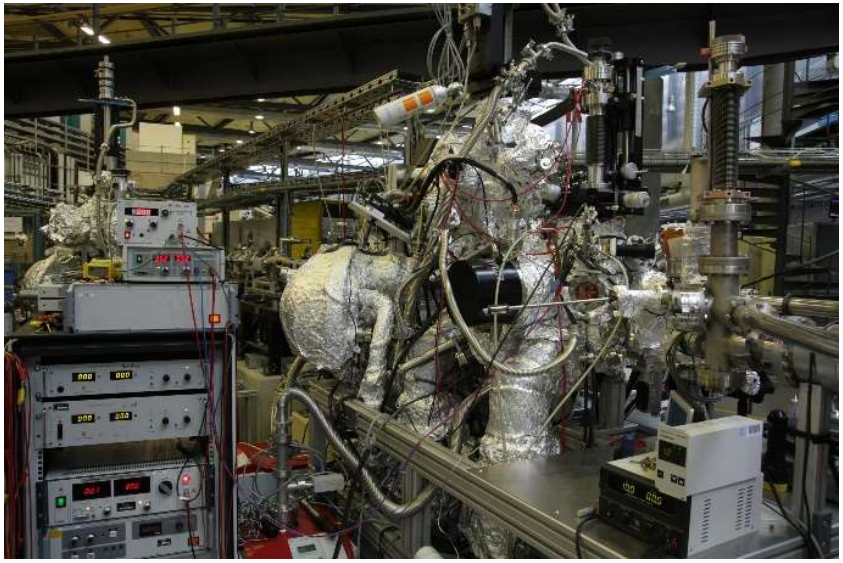

**Contact**: Anna Makarova,
anna.makarova@helmholtz-berlin.de

# Experimental station @ dipole beamline

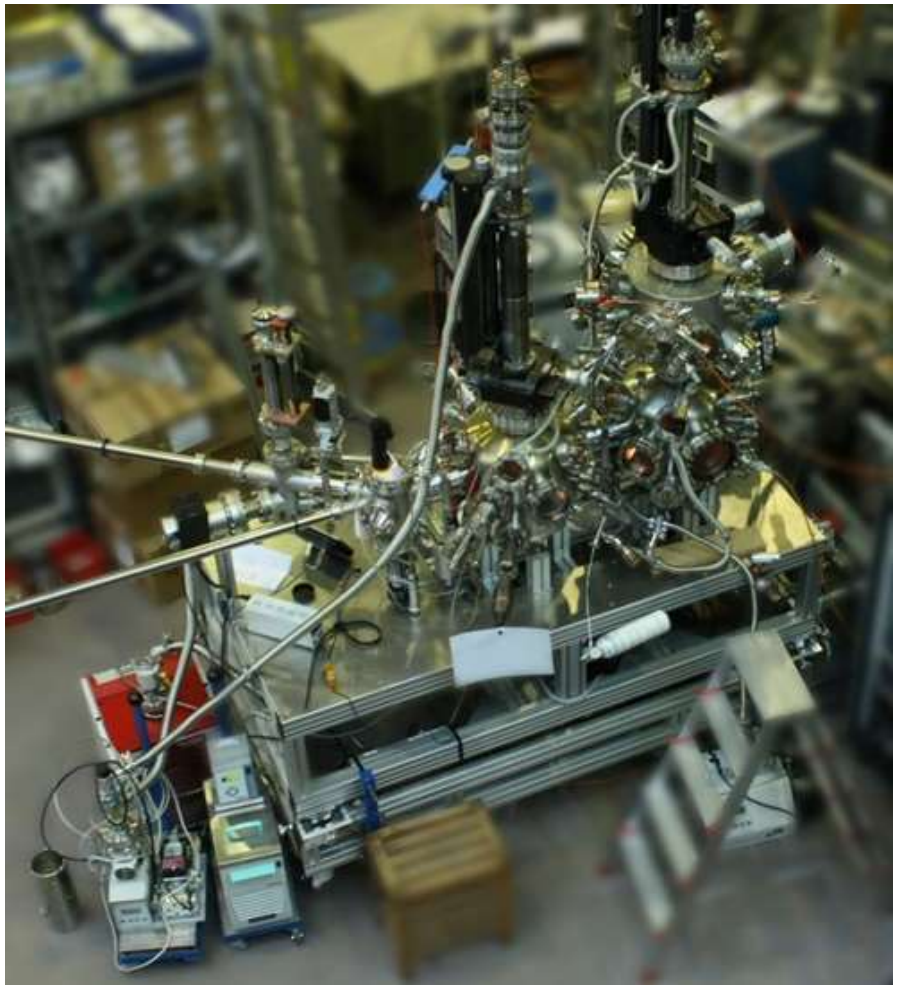

**Methods available**:

- Photoelectron Spectroscopy (PHOIBOS 150 Electron Energy Analyzer)
- Near Edge X-ray Absorption Fine Structure (NEXAFS):
  - *total electron yield, TEY (ampermeter Keithley)*
  - *partial electron yield, PEY (MCP-detector)*
  - *fluorescence yield, FY (installation of external fluorescence detector possible)*
- Low Energy Electron Diffraction
- Mass-spectroscopy (in preparation chamber)

# Experimental station @ dipole beamline

**„Maximum flexibility for user‘s experiments“**

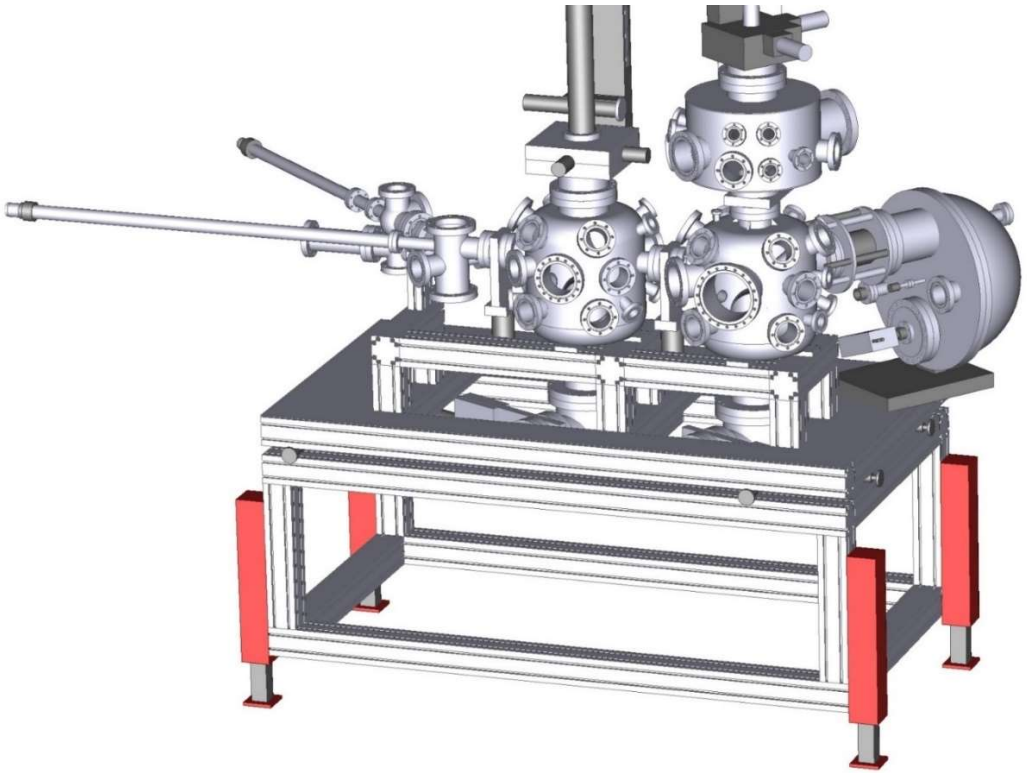

*Design: D. Marchenko, D, Vyalikh, S. Fedoseenko, C. Laubschat.*
*Installation and implementation: O. Vilkov*

**U**ltra-**H**igh **V**acuum station

- fast-entry load-lock chamber (simultaneous load of up to 8 sample holders)
- 2 preparation chambers:
  - Flash-machine
  - heating stage
  - ion gun
  - evaporators (metals, organics, etc)
  - gas inlet systems,
  - atomic hydrogen source

  etc.

✓ **cleaning of the *ex situ samples***
✓ **synthesis *in situ***
✓ **post-growth modification: study on the interactions with gases, metals, influence of heating etc.**

# Sample Environment


**Argon glove box allows transfer of the samples to the experimental station without contact with air**

# Functionalization of 2D materials

- Doping of graphene with heteroatoms

**Modulating nitrogen species via N-doping and post annealing of graphene derivatives: XPS and XAS examination**

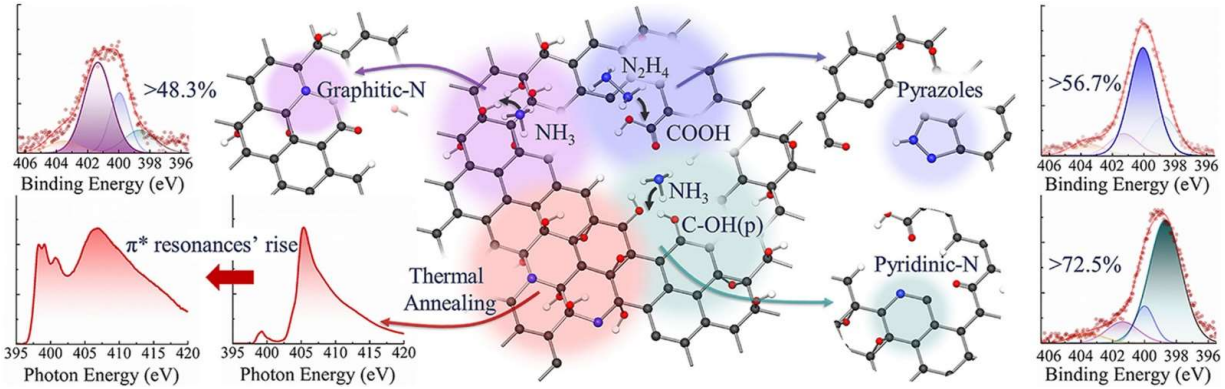


*M. K. Rabchinskii, et al., Carbon 182 (2021) 593-604*

**Nitrogen-doped graphene on a curved nickel surface**

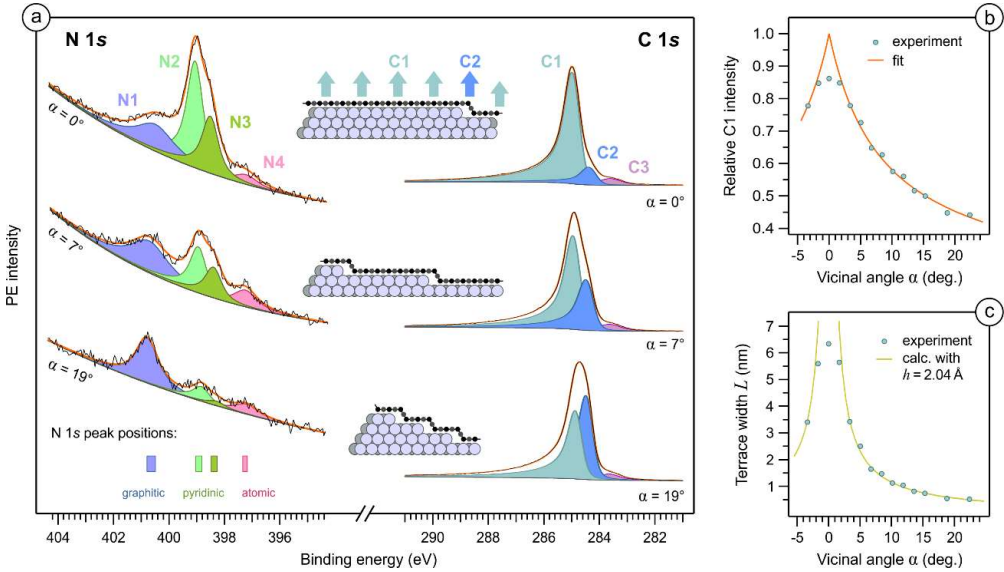


*O. Yu. Vilkov, et al., Carbon 183 (2021) 711-720*

# Stability of materials

## Nanoscale phase separation in the oxide layer at GeTe (111) surfaces

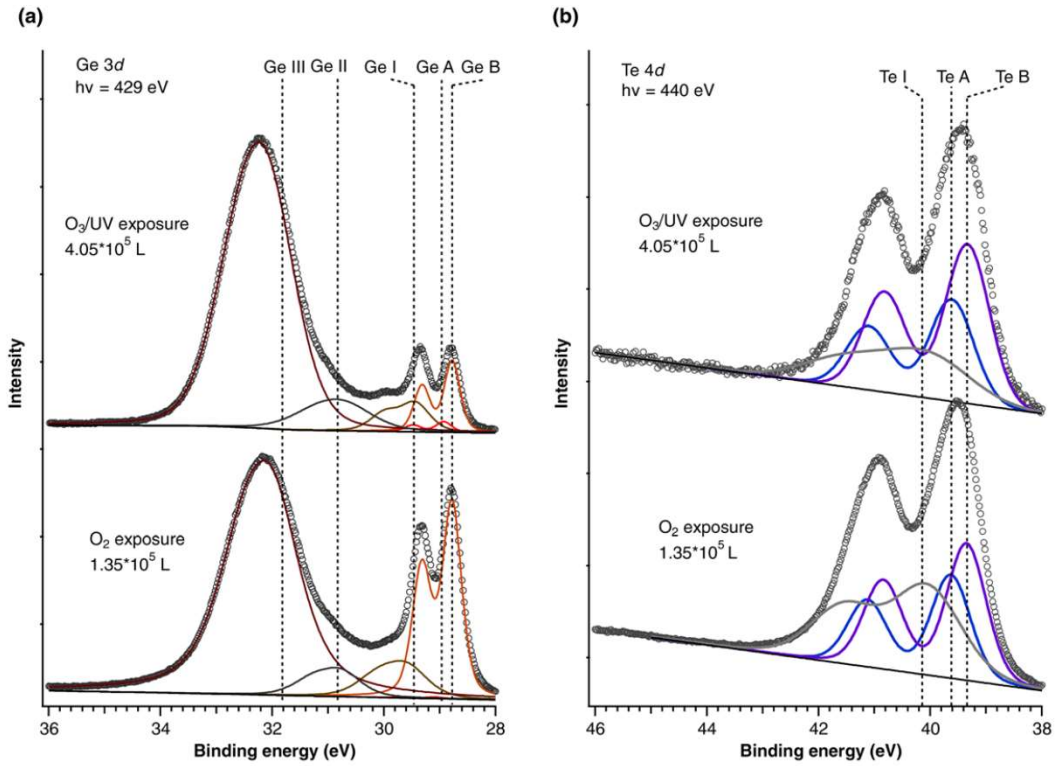


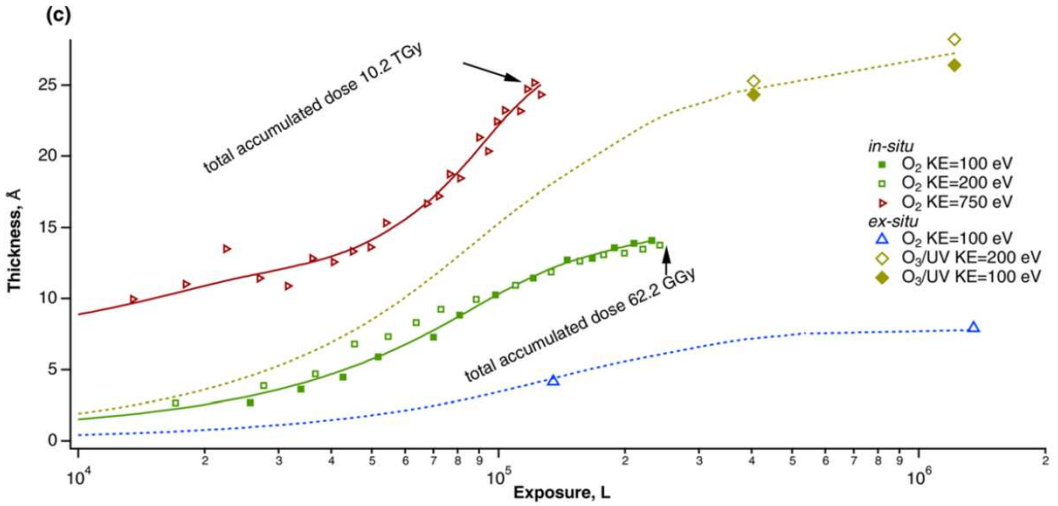


Figure: comparison of the *in situ* and *ex situ* kinetics: (a) and (b) ex situ Ge 3d and Te 4d for a GeTe (111) surface treated with molecular and atomic oxygen; (c) Reaction kinetics for the in situ data obtained at low (green) and high photon flux (brown), ex situ data obtained for molecular oxygen (blue) and in the presence of atomic oxygen (dark yellow).

*A. S. Frolov et al. Nanoscale 2022, 14, 12918*

# Energy storage materials

## A high-capacity P2 $Na_{2/3}Ni_{1/3}Mn_{2/3}O_2$ cathode material for sodium ion batteries with oxygen activity

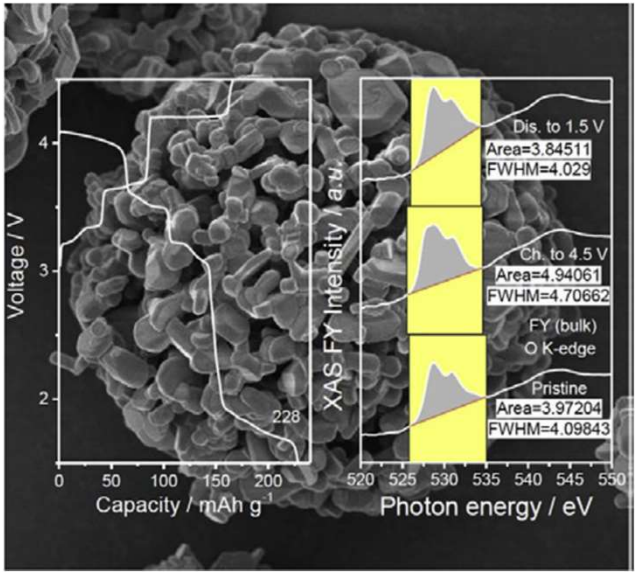


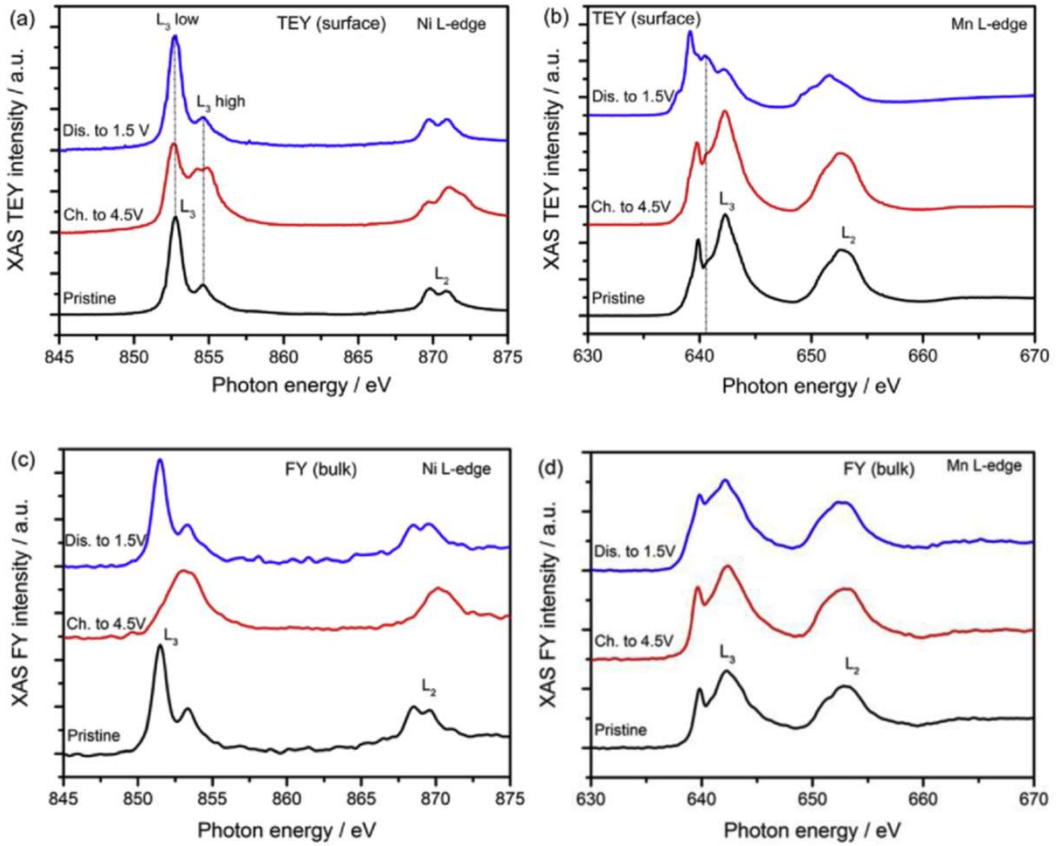


P2-$Na_xTMO_2$ materials

*T. Risthaus, et al., Journal of Power Sources 395 (2018) 16*

# Materials of biological origin

## Crystalline and amorphous calcium carbonate as structural components of the *Calappa granulata* exoskeleton

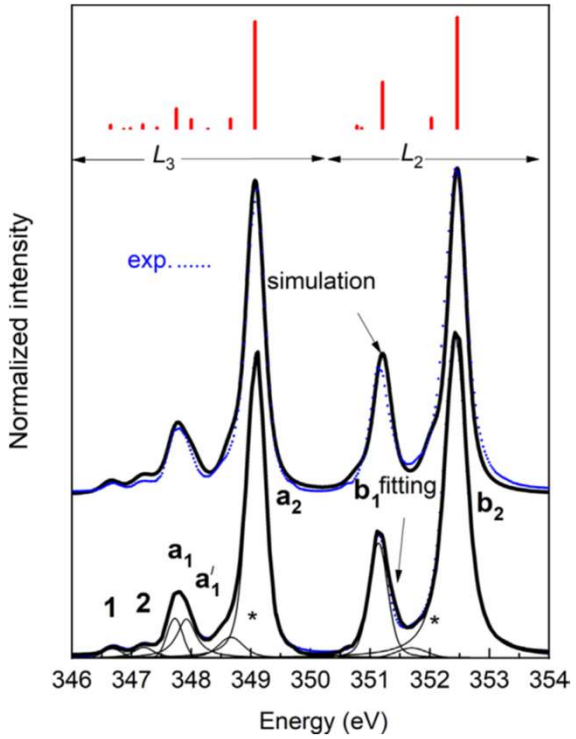


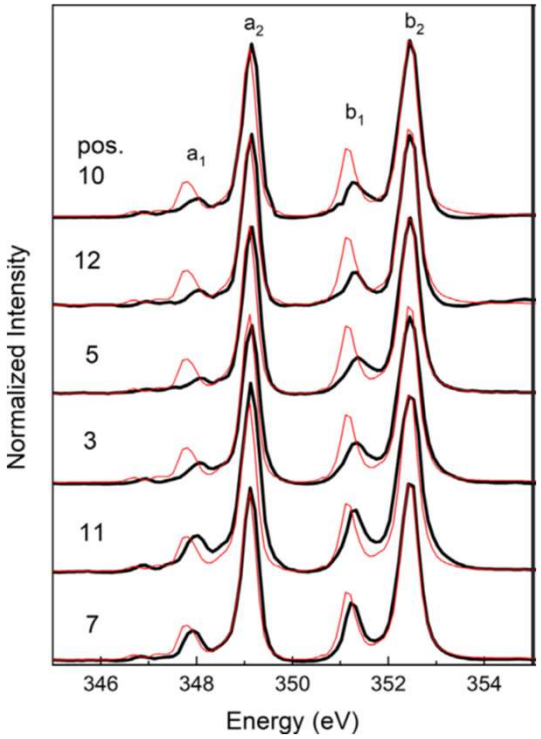


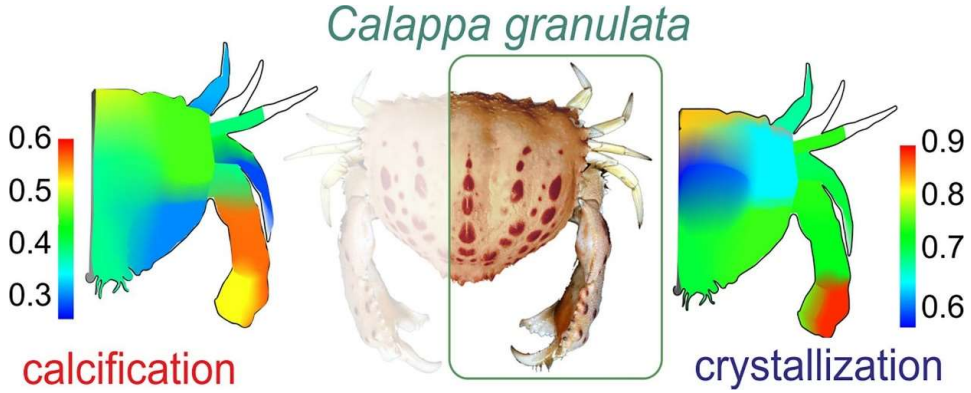


Left: Fitting and simulation of the Ca L3,2-edge NEXAFS spectrum of a crystalline calcite sample. Right: Ca L3,2-edge NEXAFS spectra recorded from various parts of the exoskeleton – black, compared with the spectrum of a calcite reference sample - red.

*M. Katsikini et al., Journal of Structural Biology, 211, 3, 2020*

# Undulator beamline U125_PGM

**Characteristics of the beamline**

| | |
|---|---|
| Energy range | 15 - 200 eV |
| Energy resolution | < 1 meV @ E < 100 eV |
| Focus size | 68 µm x 25 µm |
| Polarisation | linear |
| Endstation | fixed spin-ARPES Endstation |

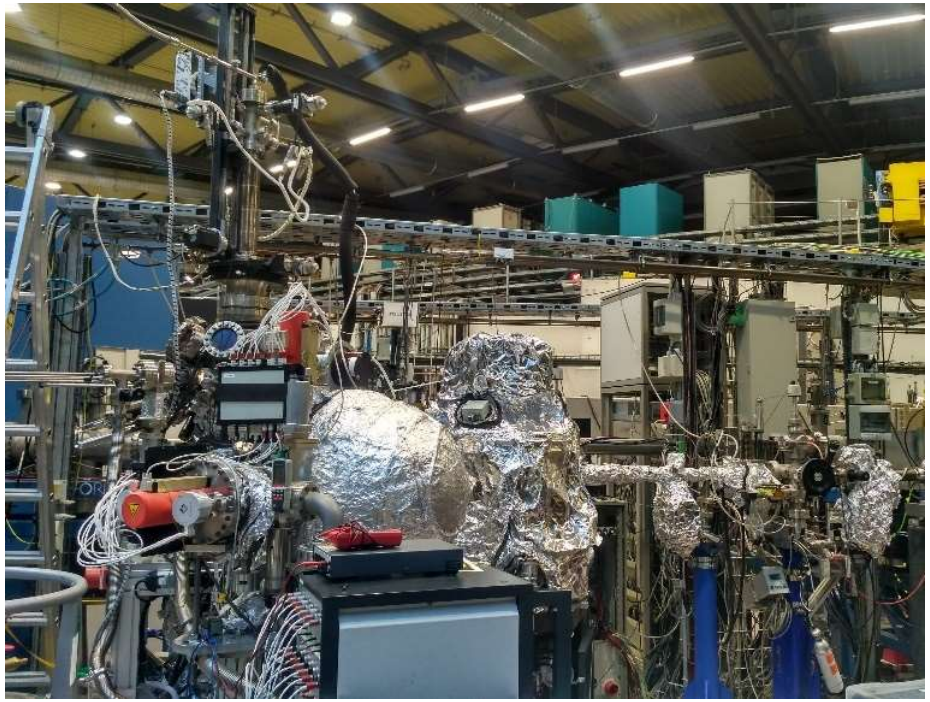

**Contact**: Jaime Sánchez-Barriga
jaime.sanchez-barriga@helmholtz-berlin.de

# Spin-ARPES endstation @ U125_PGM

Experimental station for **Spin- and Angle-resolved Photoemission**

| | |
|---|---|
| Temperature range | Measurements: 40–300 K; Sample preparation up to 2300 K |
| Pressure | UHV |
| Detector | Scienta R4000 with 2 Mott-detectors for 3D spin detection |
| Manipulator | Motorized<br>6-axes manipulator |
| Sample holders | Omicron-style |
| Additional information | Preparation chamber with<br>• heating station,<br>• sputter gun,<br>• LEED system,<br>• magnetic coil for applying external magnetic fields up to 300 Oe along any direction before measurements |

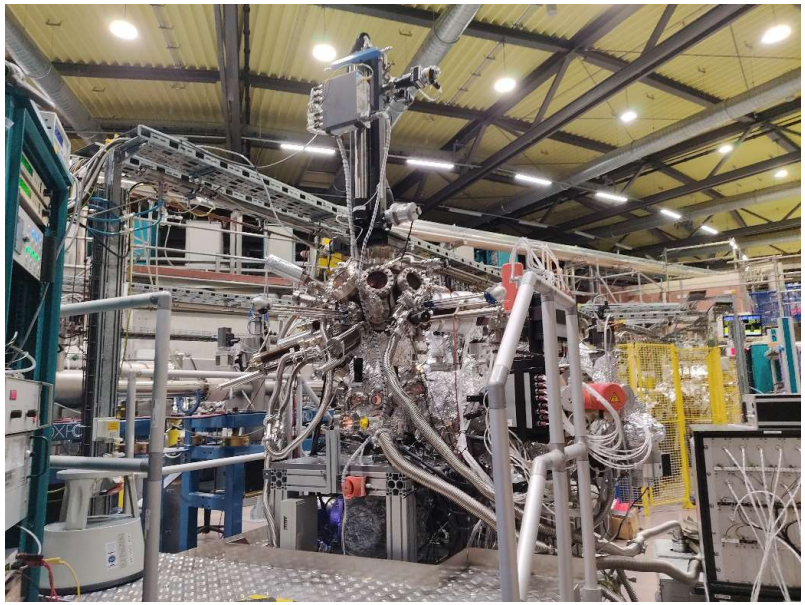

# Large magnetic gap at the Dirac point in $Bi_2Te_3/MnBi_2Te_4$ heterostructures

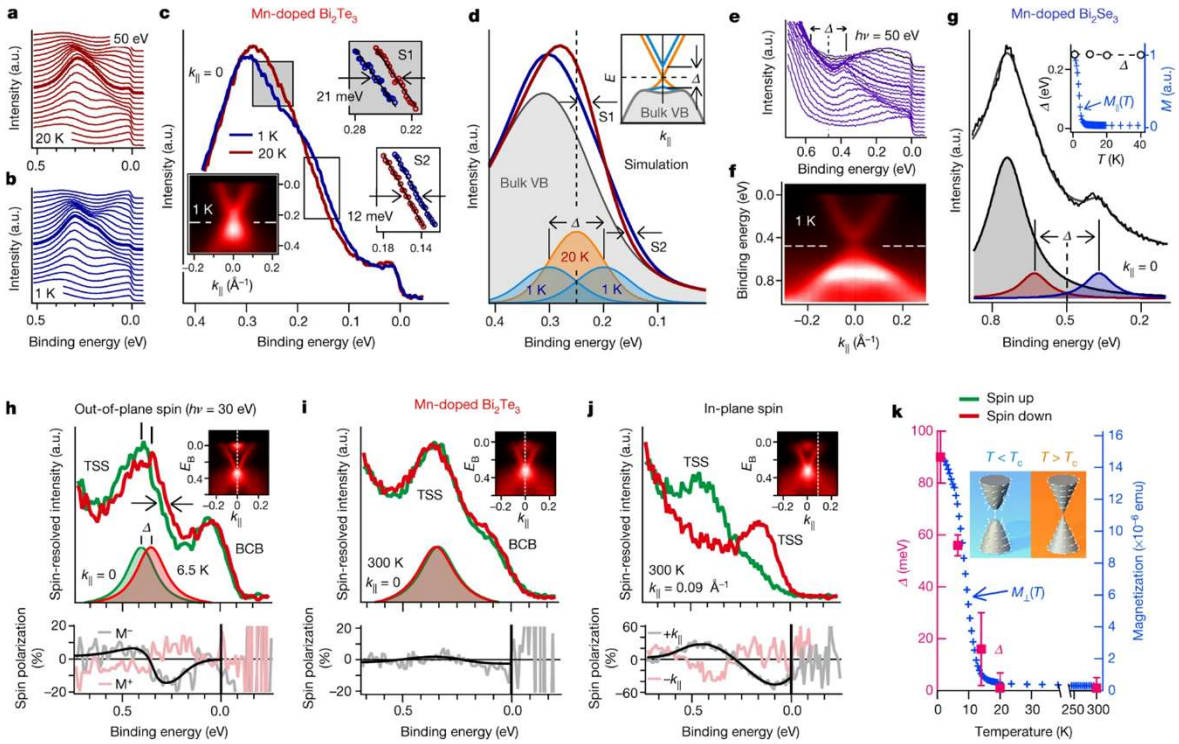


Authors use low-temperature photoelectron spectroscopy to unambiguously reveal the magnetic gap of Mn-doped $Bi_2Te_3$, which displays ferromagnetic out-of-plane spin texture and opens up only below $T_C$

*Rienks, E.D.L., et al. Nature 576, 423–428 (2019)*

# Direct Spectroscopic Evidence of Magnetic Proximity Effect in $MoS_2$ Monolayer on Graphene/Co

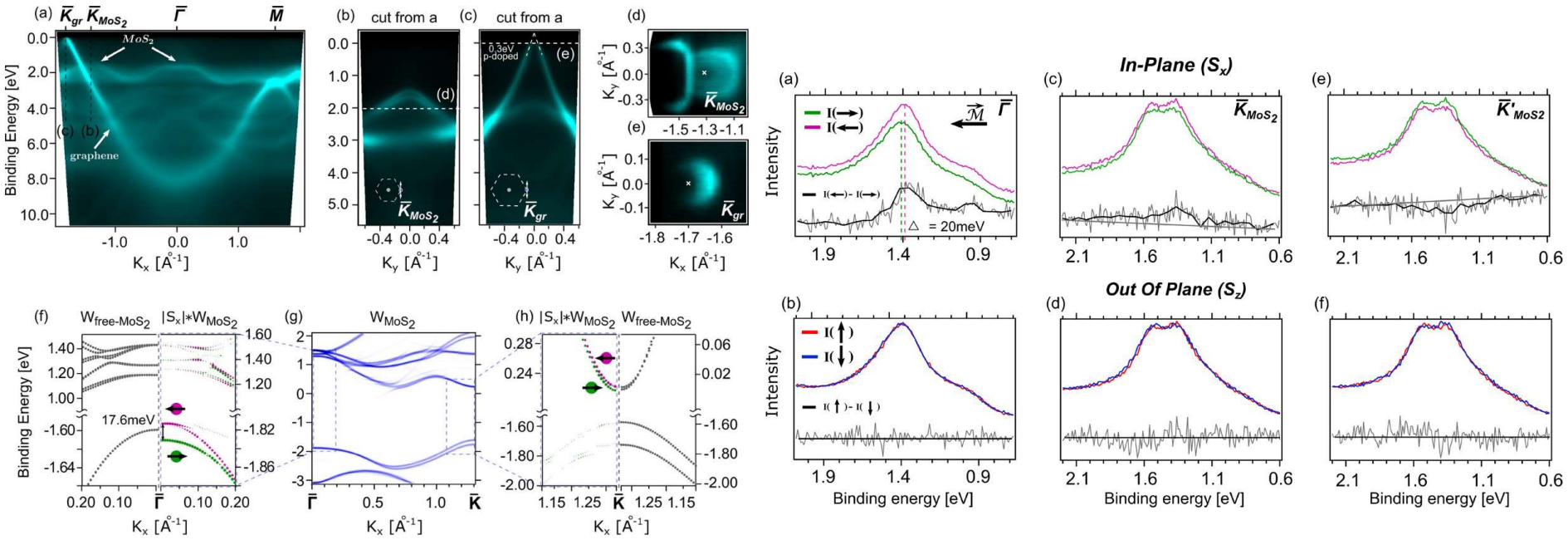


Authors demonstrate a scalable approach to the epitaxial synthesis of $MoS_2$ monolayer on a magnetic graphene/Co system. Using spin- and angle-resolved photoemission spectroscopy authors observe a magnetic proximity effect that causes a 20 meV spin-splitting at the $\overline{\Gamma}$ point and canting of spins at the $\overline{K}$ point in the valence band toward the in-plane direction of cobalt magnetization.

*V. Voroshnin et al., ACS Nano 2022, 16, 5, 7448–7456*